



A Computational Model of Dendrite Elongation and Branching Based on MAP2 Phosphorylation

TIM A. HELY*, BRUCE GRAHAM† AND ARJEN VAN OOYEN‡

*Institute for Adaptive and Neural Computation, Division of Informatics, University of Edinburgh,
5 Forrest Hill, Edinburgh, Scotland EH1 2QL, U.K.*

(Received on 27 December 1999, Accepted in revised form on 9 March 2001)

We introduce a new computational model of dendritic development in neurons. In contrast to previous models, our model explicitly includes cellular mechanisms involved in dendritic development. It is based on recent experimental data which indicates that the phosphorylation state of microtubule-associated protein 2 (MAP2) may play a key role in controlling dendritic elongation and branching (Audesirk *et al.*, 1997). Dephosphorylated MAP2 favours elongation by promoting microtubule polymerization and bundling, whilst branching is more likely to occur when MAP2 is phosphorylated and microtubules are spaced apart. In the model, the rate of elongation and branching is directly determined by the ratio of phosphorylated to dephosphorylated MAP2. This is regulated by calmodulin-dependent protein kinase II (CaMKII) and calcineurin, which are both dependent on the intracellular calcium concentration. Results from computer simulations of the model suggest that the wide variety of branching patterns observed among different cell types may be generated by the same underlying mechanisms and that elongation and branching are not necessarily independent processes. The model predicts how the branching pattern will change following manipulations with calcium, CaMKII and MAP2 phosphorylation.

© 2001 Academic Press

Introduction

The function and behaviour of the adult neuron is intrinsically tied to the structure of its dendritic arbor which forms during development. Understanding what factors determine the characteristic dendritic branching patterns will lead to an increased understanding of the functional properties of neurons. Previous computational

models of dendrite development are broadly split into two categories: statistical models which describe the structure of dendritic arbors using mathematical parameters; and models which generate branching patterns based on fundamental biological mechanisms. Statistical models (e.g. van Pelt & Verwer, 1986; Kliemann, 1987; Burke *et al.*, 1992; Tamori, 1993; Dityatev *et al.*, 1995, van Pelt *et al.*, 1997; van Pelt & Uylings, 1997) have shown that random branching events are sufficient to generate the wide variety of branching patterns observed among different cells. However, none of these models have directly clarified the cellular mechanisms involved in branching. In contrast, previous models based on biologically plausible mechanisms (e.g. Li *et al.*,

* Author to whom correspondence should be addressed.
E-mail: tim@anc.ed.ac.uk

† Current address: Department of Computing Science and Mathematics, University of Stirling, Stirling, Scotland FK9 4LA, U.K.

‡ Current address: Netherlands Institute for Brain Research, Graduate School Neurosciences Amsterdam, Meibergdreef 33, 1105 AZ Amsterdam, Netherlands.

1992; Albinet & Pelce, 1996; Hentschel & Fine, 1996) are only able to generate a limited number of dendritic geometries.

We introduce a new model which bridges the gap between these different approaches. The model is based on recent experimental data which suggest that the phosphorylation state of microtubule associated protein 2 (MAP2) plays a key role in controlling dendritic branching (Audesirk *et al.*, 1997). This supports the hypothesis put forward by Friedrich & Aszodi (1991) that MAP2 phosphorylation, which increases the spacing between microtubules, could also cause dendritic branching. In our model, the intracellular calcium concentration ($[Ca^{2+}]_i$) influences the (de)phosphorylation state of MAP2, which can switch development between elongation and branching. The current model focuses on the action of calcium as the sole determinant of MAP2 phosphorylation through the action of CaMKII and calcineurin activity. CaMKII is activated by elevated $[Ca^{2+}]_i$ levels and its activation can persist long after calcium levels have returned to their normal rest level (Giese *et al.*, 1998). Calcineurin (PP2B) is an abundant $[Ca^{2+}]_i$ and calmodulin-dependent protein phosphatase and has been estimated to comprise 1% of the total protein in the brain (Klee *et al.*, 1988). However, a wide variety of different kinases (e.g. PKA, PKC, casein-kinase II) and phosphatases (e.g. PP1, PP2A) also regulate the phosphorylated state of MAP2 either directly or indirectly (Maccioni & Cambiazo, 1995). Many of these molecules are calcium independent or only indirectly calcium dependent and in addition are regulated by downstream molecules which in turn may or may not be calcium dependent. Any molecules which affect cAMP e.g. adenylyl cyclase or phosphodiesterase will also affect PKA activity and in turn affect the phosphorylation state of MAP2 (Vallee, 1980). This is also true for the PLC-PIP2-DAG-PKC pathway (Hancock, 1997). For purposes of simplifying the current model, these interactions have not been modelled explicitly but must also be considered alongside those of CaMKII and calcineurin as factors regulating the total (de)phosphorylated state of MAP2. The model predicts that the functions relating calcium with MAP2 (de)phosphorylation determine what type of branching pattern

will occur. The results suggest that the same underlying mechanisms could control both elongation and branching in cells with diverse dendritic arbors, e.g. pyramidal and Purkinje cells, and that elongation and branching do not have to be independent, as assumed in other models (e.g. van Pelt & Uylings, 1997).

The Causes of Dendritic Branching

Branching is produced by changes in the cytoskeleton involving microtubules and actin filaments. Consequently, factors which alter microtubule dynamics have a significant effect on dendritic branching. The MAP family of proteins regulate many factors of microtubule dynamics, including (de)polymerization, bundling, spacing, and interaction with actin filaments (for an extensive review see Maccioni & Cambiazo, 1995). MAP2 is primarily found in dendrites and has been suggested to play a role in microtubule bundling (Lewis *et al.*, 1989). A decrease in microtubule bundling may be related to the appearance of dendritic arborization. The phosphorylation state of MAP2 alters its interactions with microtubules and also with actin filaments (Selden & Pollard, 1983). Microtubule assembly and/or stability is increased when MAP2 is dephosphorylated (Yamamoto *et al.*, 1985). In developing hippocampal cultures, an exponential increase in dendritic arborization correlates with an exponential increase in MAP2 phosphorylation, but not with the total amount of dephosphorylated MAP2, or the overall neurite length (Diez-Guerra & Avila, 1993). In lamprey central neurons, microtubule destabilization and MAP2 phosphorylation precedes dendritic sprouting (Hall *et al.*, 1991). Ca^{2+} /calmodulin-dependent protein kinase II (CaMKII) affects phosphorylation of microtubule-bound MAP2 and so disrupts microtubule bundling (Lewis *et al.*, 1989). Further experimental support for a role of CaMKII in dendrite branching was provided recently when it was found that inhibitors of CaM kinases reduced dendrite branching to as little as 30% of control values (Audesirk *et al.*, 1997), whilst agents that increased protein phosphorylation increased dendritic branching by up to 200%. MAP2 dephosphorylation is controlled by agents such as

the phosphatase calcineurin (also known as PP2B) (Hancock, 1997).

The combined experimental data suggest that the (de)phosphorylation of MAP2 in dendrites by calcineurin and CaMKII affect microtubule stability and growth and may play a key role in switching neurite development between elongation and branching. As both CaMKII and calcineurin are calcium dependent, changes in $[Ca^{2+}]_i$ concentration will also affect neurite elongation and branching. Therefore, the key variable in our new model of branching and elongation is the phosphorylation state of MAP2 in the growing dendritic terminals.

The Model

COMPARTMENTAL MODEL

The developing neuron is described by a simple compartmental model which initially has two compartments: a spherical soma of radius R_{soma} and a single, short, cylindrical dendrite of length L and radius R [see Fig. 1(a)]. Growth of the neurite through time involves elongating and subdividing terminal compartments and bifurcating terminal compartments into two daughter compartments when branching occurs. Each compartment contains a

particular concentration of intracellular calcium (model parameter Ca) and MAP2 that may change over time. The concentrations in the terminal compartments determine the rate of elongation and branching. To simplify the current simulations, it was assumed that tubulin dimers are not a limiting factor in outgrowth and transport and gradients of tubulin dimers were not modelled explicitly. (In related “cell pulling” experiments carried out by Dennis Bray, axonal outgrowth rates of up to $100 \mu\text{m hr}^{-1}$ were achieved and tubulin dimer availability was not a limiting factor, Bray, 1984). The model simulates the growth of the dendritic tree in discrete time steps, dt . New compartments of length dx are added as the dendrite elongates by subdividing terminal compartments when they reach length $2dx$ [see Fig. 1(b)]. This approximates continuous outgrowth with discrete compartments. At each time step a terminal compartment may also branch with a probability determined by the concentration of Ca and the phosphorylation state of MAP2. When branching occurs the terminal compartment is replaced by two new daughter compartments of reduced diameter and length, L , set such that the volume of the original terminal compartment is preserved [see Fig. 1(c)]. A simulation is stopped after a given

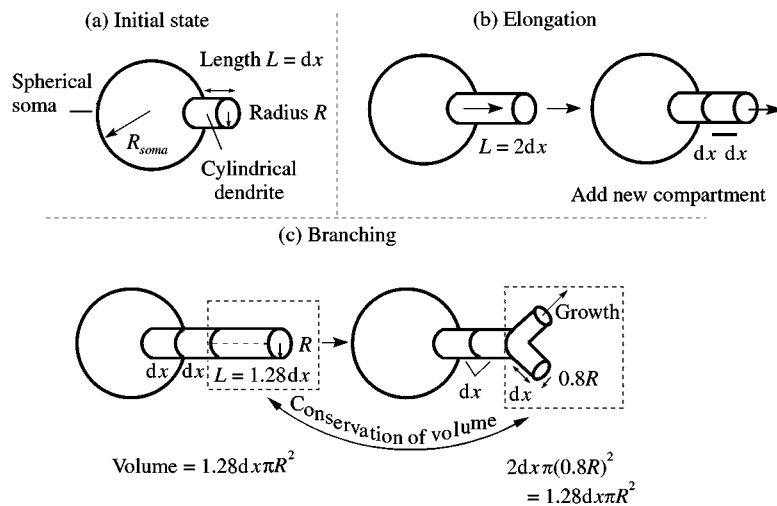


FIG. 1. The compartmental model. (a) Initial state, (b) new compartments are added when the length of the terminal compartment reaches twice dx . (c) Branching involves the redistribution of the terminal compartment volume into two new compartments. The radius of the two daughter dendrites is equal to a fixed fraction of the parent dendrite radius (default: 0.8). The initial length of the terminal compartments is set to satisfy the conservation of volume.

length of time and the characteristics of the dendritic arbor are noted.

MAP2 (DE)PHOSPHORYLATION

The concentrations in each compartment of Ca and different forms of MAP2 are determined by the reaction scheme shown in Fig. 2. The rates of change of Ca, unbound MAP2 ($MAP2_u$), dephosphorylated MAP2 that is bound to microtubules ($MAP2_b$) or bound and phosphorylated MAP2 ($MAP2_p$) in each individual compartment are given by the following four differential equations. The concentrations of microtubule polymer and calmodulin/CaMKII protein are not modelled explicitly.

$$\frac{\partial Ca}{\partial t} = D_{Ca} \frac{\partial^2 Ca}{\partial x^2} + I - \delta_{Ca} Ca \quad (1)$$

= diffusion + influx - decay,

$$\frac{\partial MAP2_u}{\partial t} = D_u \frac{\partial^2 MAP2_u}{\partial x^2} + P - c_1 MAP2_u$$

+ c₂MAP2_b - δ_uMAP2_u

$$= \text{diffusion} + \text{prodn}$$

- rate to/from MAP2_b - decay,

(2)

$$\frac{\partial MAP2_b}{\partial t} = c_1 MAP2_u - c_2 MAP2_b - c_3 F MAP2_b$$

= + c₄GMAP2_p - δ_bMAP2_b

= rate to/from MAP2_u

- (de)phosph. to/from MAP2_p

- decay = 0,

(3)

$$\frac{\partial MAP2_p}{\partial t} = c_3 F MAP2_b - c_4 G MAP2_p$$

- δ_pMAP2_p

= (de)phosphorylation to/from MAP2_b

- decay

(4)

Only the concentrations of Ca and unbound MAP2 ($MAP2_u$) are calculated dynamically. $MAP2_b$ and $MAP2_p$ are assumed to be at quasi-steadystate at each time step. This allows the concentration of $MAP2_b$ and $MAP2_p$ to be directly calculated from the concentration of Ca and

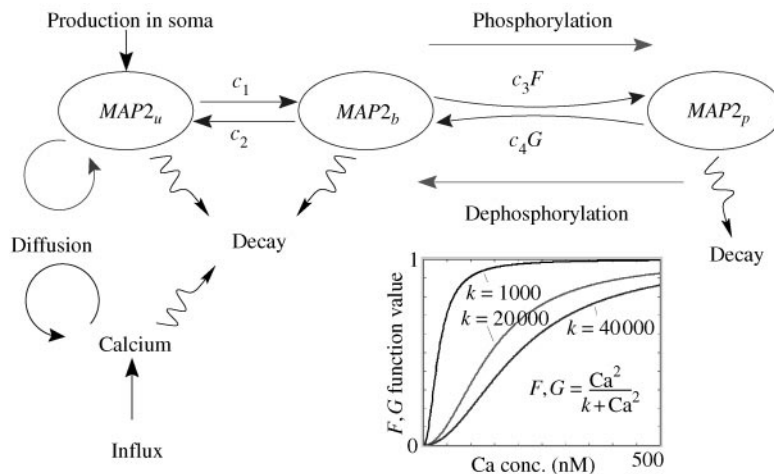


FIG. 2. The cell dynamics simulated in the branching model. Diffusible $MAP2_u$ is produced in the soma and is converted into the microtubule-bound $MAP2_b$ complex and then phosphorylated into $MAP2_p$. Calcium enters across the membrane and diffuses throughout the dendrite. The calcium-dependent functions F, G control the on/off rate of phosphorylation. The shape of these functions is shown for various values of the steepness parameter k used in the simulations.

$MAP2_u$. $MAP2_u$ is produced in the soma at a constant rate P (P is zero elsewhere). To model the calcium gradient observed in growing dendrites (Hentschel & Fine, 1996), there is a small net influx I of calcium across the membrane at a rate proportional to the surface-to-volume ratio of each compartment. Ca and $MAP2_u$ diffuse throughout the dendrite with rates D_{Ca} and D_u , respectively. $MAP2_u$ conversion into $MAP2_b$ is governed by rate constants c_1 and c_2 ; $MAP2_b$ conversion into $MAP2_p$ is calculated using c_3, c_4 and the calcium-dependent phosphorylation function $F = Ca^2/(k_F + Ca^2)$ and dephosphorylation function $G = Ca^2/(k_G + Ca^2)$. These functions have the sigmoidal shape shown in Fig. 2 and saturate towards an upper limit. (k_F, k_G control the steepness of the slope of these curves.) Saturation reflects the finite amount of MAP2 and CaMKII complex found within the dendrites. Calcium buffering is not modelled explicitly although the low Ca diffusion rate incorporates a high buffering effect. Removal of Ca through decay (δ_{Ca}) is also dependent on the Ca-concentration. Finally, δ_u, δ_b and δ_p determine the decay rates of different states of MAP2.

The equations were solved using first-order Euler integration with a fixed time step dt ($dt < dx^2/2D$ to ensure diffusive stability (Press *et al.*, 1988)).

ELONGATION AND BRANCHING

At each time step the elongation rate and branching probability of each dendritic terminal compartment are calculated. The simulation was initially run for 10 000 time steps without any elongation to eliminate any start up effects and to ensure that the system was at equilibrium before elongation began. The rate of elongation is proportional to the ratio of bound to dephosphorylated MAP2, $MAP2_b/MAP2_p$. In contrast, the probability that a terminal compartment branches into two daughter segments in any given time step is proportional to the inverse ratio, $MAP2_p/MAP2_b$. These ratios are multiplied by the absolute values of $MAP2_b$ and $MAP2_p$, respectively, to reflect the fact that a physical amount of MAP2 is required for elongation or branching to occur. The actual probability that a terminal segment branches in one

time step, dt , is the product of the branching probability per unit length, P_{br} , and the elongation, E , during that time step, where

$$E = E^0 \times k_E \times MAP2_b \frac{MAP2_b}{MAP2_p} \quad (\mu\text{m s}^{-1}), \quad (5)$$

$$P_{br} = P_{br}^0 \times k_B \times MAP2_p \frac{MAP2_p}{MAP2_b} \quad (\mu\text{m}^{-1}). \quad (6)$$

Constants k_E and k_B ensure that the initial elongation rate is E^0 , and the initial branching probability per unit length is P_{br}^0 .

As demonstrated by the results presented below, these equations allow a range of elongation speeds and branching rates. If both $MAP2_b$ and $MAP2_p$ have equally high concentrations, rapid branching and outgrowth will occur simultaneously. Conversely, slow growth and branching take place at low concentrations.

Results

Though the model is apparently complex, neurite development is effectively controlled by only two dynamic variables: the intracellular calcium concentration (Ca) and the concentration of unbound MAP2 ($MAP2_u$) in the growing terminals. The following results demonstrate how widely varying tree topologies can be generated by manipulating the rate functions, F and G , that control the Ca-dependent phosphorylation and dephosphorylation of MAP2. The model is also able to reproduce the characteristics of a specific data set obtained from rat pyramidal basal dendrites (Larkman, 1991).

DIFFERENT TREE GEOMETRIES

Figure 3(a-c) shows the time course of development of three characteristic dendritic arbors produced by the model. As can be seen, a wide range of different geometries can be produced, ranging from trees with long proximal segments and heavily branched, short outer segments to trees where the segment length increases distally. In Fig. 3(a) and (b), the relative lengths of proximal and distal segments bear comparison with real dendrites, rather than the absolute lengths.

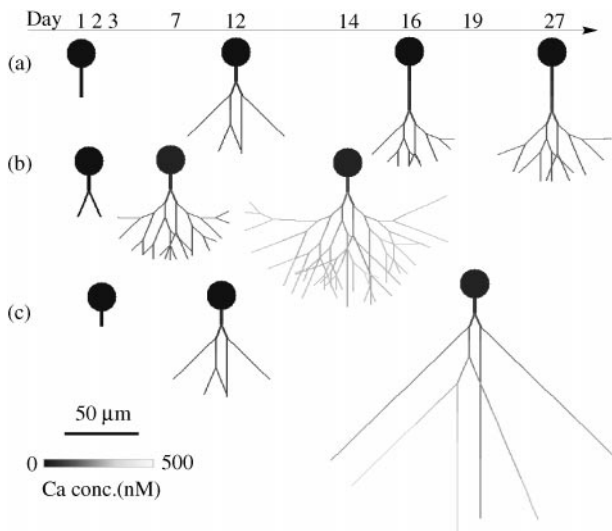


FIG. 3. Dendritic arbors produced by the model. This model is able to generate a wide range of dendrites by varying the (de)phosphorylation reaction rates c_3 , c_4 and parameters k_F , k_G which alter the shape of the (de)phosphorylation functions F and G . In (a) the branch probability is low initially ($0.015 \mu\text{m}^{-1}$) and increases with time. In (b) the branching probability ($0.2 \mu\text{m}^{-1}$) is approximately constant throughout. In (c) the branching probability is initially high ($0.6 \mu\text{m}^{-1}$) and falls off rapidly as the dendrite grows. The basic parameter values are: $dx = 10 \mu\text{m}$, $dt \approx 40 \text{ s}$, $R_{\text{soma}} = 10 \mu\text{m}$, initial dendrite $R = 1 \mu\text{m}$, $E^0 = 2^{-4} \mu\text{m s}^{-1}$, $[\text{Ca}]^0 = 30 \text{ nM}$, $D_{\text{Ca}} = 10^{-8} \text{ cm}^2 \text{ s}^{-1}$, $I = 0.01 \text{ nM } \mu\text{m}^{-1} \text{ s}^{-1}$, $\delta_{\text{Ca}} = 10^{-4} \text{ s}^{-1}$, $\text{MAP2}_u^0 = 10$, $D_u = 10^{-8} \text{ cm}^2 \text{ s}^{-1}$, $P = 0.003 \text{ s}^{-1}$, $c_1 = 0.95$, $c_2 = 0.05$, $c_3 = c_4 = 0.8$, $\delta_{u,b,p} = 10^{-5} \text{ s}^{-1}$, $k_F = k_G = 1000$. In (a) $c_4 = 0.2$, $k_F = 20\,000$, $E^0 = 5 \times 10^{-5} \mu\text{m s}^{-1}$; in (c) $c_3 = 0.2$, $k_G = 40\,000$, $E^0 = 4 \times 10^{-4} \mu\text{m s}^{-1}$.

In Fig. 3(c), the dendritic length has been matched to experimental data from rat pyramidal basal dendrites (Larkman, 1991).

Figure 3(a) shows the type of dendritic branching pattern observed in cultured hippocampal neurons (Diez-Guerra & Avila, 1993). In this simulation, the initial branching probability is low because at low Ca concentrations dephosphorylation is greater than phosphorylation ($k_F = 20\,000 > k_G = 1000$, see Fig. 2). As the tree grows, increases in the distal Ca concentration cause increased MAP2 phosphorylation, which leads to an increased branching probability amongst distal dendrites. The Purkinje cell is an extreme example of a cell which might employ this type of branching mechanism (although external factors also play a significant role in its development; Schilling *et al.*, 1991).

Figure 3(b) shows the typical branching structure produced when the branching probability and elongation rate remain approximately constant throughout the simulation. In this case the (de)phosphorylation constants are equal ($k_F = k_G = 1000$). The ratio $\text{MAP2}_b/\text{MAP2}_p$ remains constant and the elongation and branching rates are unaffected by distal increases in Ca concentration. Both the rate of elongation and the branching probability do, however, decrease slowly with increasing distance from the soma due to a lack of available MAP2.

COMPARISON WITH BIOLOGICAL DENDRITES

Figure 3(c) shows the dendritic arbor generated by the model when simulating the basal dendrites of a rat pyramidal neuron. There are a small number of terminal segments (average six) which are over 6 times as long as the proximal segments. The form of the functions which model the effect of calcium on MAP2 (de)phosphorylation determines the type of dendritic arbor generated. In contrast to Fig. 3(a), in this simulation the (de)phosphorylation parameters ($k_G = 40\,000 > k_F = 1000$, see Fig. 2) promote branching and inhibit elongation at low Ca concentrations. The increased Ca concentration in distal dendrites leads to an increase in the rate of MAP2_p dephosphorylation and in the ratio of $\text{MAP2}_b/\text{MAP2}_p$. Thus, the elongation rate increases and the branching probability decreases as the tree grows. This results in longer distal dendrites and a larger overall dendritic tree than in either Fig. 3(a) or (b).

In order to quantify the type of dendritic arbor produced, a number of features are standardly used to determine the characteristic properties of the arbor (van Pelt & Uyling, 1997). These include the total number of terminals per dendritic branch (also called the degree of the dendrite) and the asymmetry of the tree structure as measured by the asymmetry index A_r . This index varies between zero for symmetric trees to one for maximally asymmetric trees [see van Pelt & Uylings (1997) for the mathematical definition]. Other features include the intermediate and terminal segment lengths, total segment length and path-lengths from the soma to distal tips. Many biological neuronal tree types can be distinguished by

TABLE 1
Comparison between dendritic tree characteristics of MAP model and of rat basal dendrite data (mean ± S.D)

| Shape variables | Biological data | Simulation data |
|----------------------|-----------------|-----------------|
| Degree* | 6.0 ± 2.7 | 5.99 ± 2.1 |
| Asymmetry† | 0.38 ± 0.22 | 0.39 ± 0.20 |
| Total length‡ | 777 ± 342 | 749 ± 306 |
| Terminal length* | 117 ± 33 | 107 ± 31 |
| Intermediate length* | 15.4 ± 13.4 | 22.4 ± 19.5 |
| Pathlength* | 156 ± 29 | 161 ± 15 |

*Larkman (1991).
 †van Pelt *et al.* (1992).
 ‡van Pelt & Uylings (1997).

the mean and distribution of these parameters (van Pelt *et al.*, 1997; van Pelt & Uylings, 1997).

Amongst the best characterized tree type is the rat pyramidal cell basal dendrite (Larkman, 1991; van Pelt & Uylings, 1997). Table 1 compares the average values of the tree characteristics obtained from 150 simulation runs using the parameters as for Fig. 3(c), with the biological data. It can be seen that the mean and standard deviation of the simulated tree characteristics closely match those of the biological data set. The full set of results produced by the MAP2 simulation is plotted in histogram format in Fig. 4. This can be compared to the results produced by the statist-

ical BESTL model (van Pelt & Uylings, 1997) when its parameters were optimized for the data from rat pyramidal cell basal dendrites. These results were reproduced in an equivalent simulation of the BESTL model by Graham *et al.* (1998).

Discussion

This is the first model to simulate dendritic branching patterns based on $[Ca^{2+}]_i$ regulation of the relative phosphorylation state of MAP2. In contrast to previous models, neurite branching and elongation are controlled by the same underlying mechanism. This occurs through dynamic changes in the ratio of dephosphorylated to phosphorylated MAP2 caused by a distally increasing $[Ca^{2+}]_i$ concentration. This simultaneously controls the elongation rate and branching probability. The model is able to generate a variety of dendritic branching patterns which have a high similarity to the characteristics of biological arbors. These include dendrites where branching increases distally (cf. cultured hippocampal neurons, Diez-Guerra & Avila, 1991) and dendritic trees with elongated distal dendrites (pyramidal neuron basal dendrites). This suggests that cells with different dendritic geometries, such as pyramidal and Purkinje cells, may use the same fundamental elongation and branching mechanisms during development but

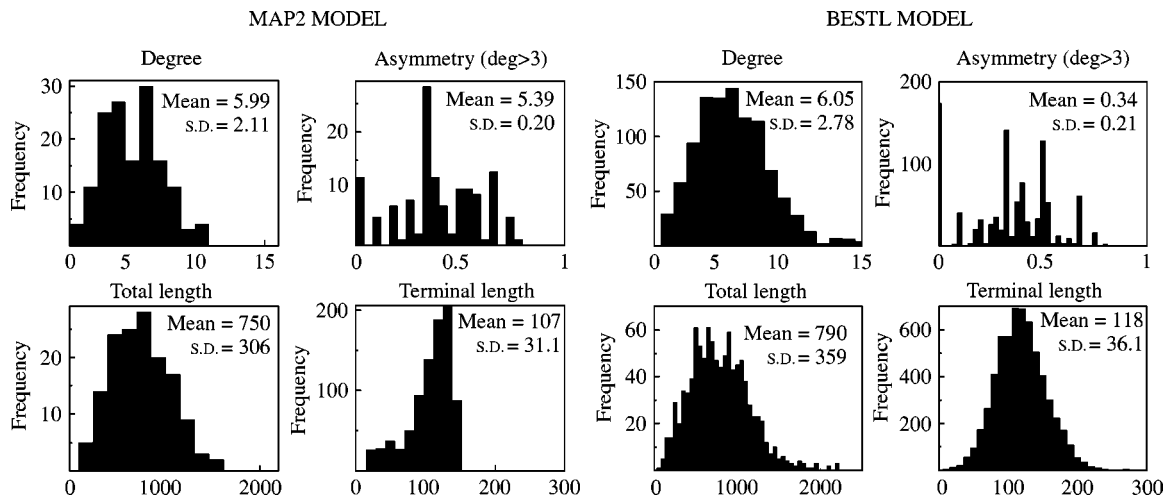


FIG. 4. Characteristic topologies of dendritic trees generated by the MAP2 model compared to the BESTL model.

with different “parameter” settings. One critical parameter setting may be the calcium setpoint level for a particular cell (Mattson & Kater, 1987).

The current model focuses on the action of $[Ca^{2+}]_i$ as the sole determinant of MAP2 phosphorylation through CaMKII and calcineurin interactions. In reality, a wide variety of kinases and phosphatases (de)phosphorylate MAP2 (for a thorough review see Maccioni & Cambiazo, 1995). This is undoubtedly an over-simplification of the model, however, the results show that a $[Ca^{2+}]_i$ -dependent mechanism alone has the potential to control the outgrowth and branching process.

Similarly, we have concentrated on the role that microtubule dynamics and in particular MAP2 may play in dendrite development. The actin filament (F-actin) network also plays a major role in governing growth cone morphology and behaviour. MAP2 can interact with actin filaments and increased phosphorylation inhibits the actin filament cross-linking activity of MAP2 (Selden & Pollard, 1983). Calcium influx also has a major effect on actin bundle dynamics and retrograde flow rates (Welnhofer *et al.*, 1999). The F-actin network is not explicitly simulated in the model and again this is an over-simplified representation of the branching process. However, the results show that microtubule dynamics could directly control the shape of the developing dendritic tree.

In the model, the size and degree of the dendritic arbor is primarily affected by the initial elongation and branching rates. The constants k_F and k_G , which control the slope of the MAP2 (de)phosphorylation functions F and G , are also important as they determine whether branching is promoted or inhibited as the dendrite grows and the calcium concentration increases distally. The sigmoidal form of the functions F and G is not crucial for this effect on branching. For example, a wide range of tree topologies can be generated if F and G are linear functions, rather than sigmoidal. By varying the starting value and slope of linear functions the (de)phosphorylation ratio F/G can either increase, decrease or remain constant with increasing calcium concentration. However any MAP2 phosphorylation by CaMKII at high calcium concentrations will largely

be cancelled out by dephosphorylation due to calcium-dependent phosphatases such as calcineurin. For this reason we used saturating (sigmoidal) (de)phosphorylation functions. The relative rates of CaMKII vs. calcineurin activity as a function of $[Ca^{2+}]_i$ are not well known. However, the model predicts that if MAP2 and $[Ca^{2+}]_i$ are involved in generating branching patterns, then the dependence of phosphorylation and dephosphorylation should be of the form used here. The exact shape of the functions has yet to be determined experimentally but this would allow the predictions of the model to be tested.

The surface-to-volume ratio of branches has a great influence on the local $[Ca^{2+}]_i$ concentration. In the model $[Ca^{2+}]_i$ increases distally in the growing tree due to the increasing surface-to-volume ratio in newly branched dendrites with smaller diameters than their parents. The reduction factor of 0.8 from parent to daughter diameters at a branch point was used exclusively here and matches the proximal-to-distal diameter reduction from 2 to 1 μm over an average of three branch points, seen in rat pyramidal cell basal dendrites. A distal decrease in diameter is representative of most dendritic tree types and the rate of decrease will affect the rate of increase in distal calcium. The branching patterns (for parameters used in current simulations) would be different in a developmental scenario where the terminal branches have fixed diameters and the diameters of proximal (parent) segments increase. However, under these conditions, a calcium gradient would also be generated with higher concentrations towards the periphery.

The actual free $[Ca^{2+}]_i$ concentration within dendritic compartments varies widely between cell types and different *in vitro* preparations. The rest levels of cytoplasmic free calcium measured with Fura-2 in cultured Purkinje cells in Krebs saline is 85 and 142 nM at 5 and 14 days *in vitro* (DIV). In growth medium, however, the rest level is over 250 nM at 5DIV and this increases to a rest level of around 393 nM at 14DIV (Schilling *et al.*, 1991). In chick dorsal root ganglion neurons, $[Ca^{2+}]_i$ resting levels are around 42 nM but rise to 142 nM during outgrowth on laminin. Individual filopodia with rest levels of $[Ca^{2+}]_i > 100$ nM can

have sustained increases in $[Ca^{2+}]_i$ of up to and over 400 nM (Kuhn *et al.*, 1998). For the particular parameter settings used to generate the cell shown at 19DIV in Fig. 3(c) the $[Ca^{2+}]_i$ concentration in distal dendritic compartments is at the upper end of values observed biologically during neurite outgrowth (over 400 nM). The addition of calcium buffering mechanisms would lower the $[Ca^{2+}]_i$ rest level but this would not significantly affect the morphologies that could be generated.

The steepness of the concentration gradients of Ca and $MAP2_u$ along a dendritic branch depends on their rate of transport relative to the elongation rate. Transport of calcium through the cytoplasm is greatly affected by interaction with negatively charged particles and various buffering processes. As a result, the effective diffusion coefficient for $[Ca^{2+}]_i$ (10^{-8} – 10^{-7} $cm^2 s^{-1}$) is around 100 times lower than for calcium diffusion in water (6×10^{-6} $cm^2 s^{-1}$) (Pelce, 1993). Transport of $MAP2_u$ is a combination of diffusion over short distances (up to 200 μm) coupled with slow active transport. This combination has been simply modelled as a slow diffusional process [cf. van Veen & van Pelt (1994), where transport of tubulin is modelled similarly]. Increasing the rate of $MAP2_u$ or calcium diffusion leads to shallower concentration gradients. This also occurs by increasing the size of the soma as a large cell will have a greater buffering capacity than a small one. With rapid diffusion, any distal increase in $[Ca^{2+}]_i$ concentration would be buffered by the soma which acts as a sink. In the limit this would lead to constant rates of elongation and branching.

The model is able to capture the overall characteristics of rat pyramidal neuron basal dendrites (Larkman, 1991). Although the mean and standard deviation of the dendrite asymmetry of the simulated trees match the biological values (Table 1), the model generated significantly fewer symmetric trees (see Fig. 4). There should be a tendency to produce symmetric trees if the probability of branching in a newly branched dendrite is lower than in unbranched dendrites. In the simulations of the rat basal dendrites, increased branching occurs at lower $[Ca^{2+}]_i$ levels. Newly branched dendrites have higher $[Ca^{2+}]_i$ levels due to the increase in the ratio of

surface area to volume caused by the reduction in dendrite diameter following branching. As a result a larger, unbranched dendrite is slightly more likely to branch than a newly branched dendrite. The shallow gradient in dendrite diameter used here evidently produces only a small bias towards symmetrical trees. The simulated dendrites also fail to produce the population of extremely long terminal segments ($> 150 \mu m$) observed in real cells (Fig. 4). The model dendrites were generated in a single simulation run without modifying any parameters. To reproduce the terminal length data using the BESTL model required using separate branching and elongation phases with different rates of elongation in each phase (van Pelt & Uylings, 1997). In contrast, our model generates elongation and branching from the same intrinsic mechanism so the rate of elongation cannot be manipulated independently. The simulations were also performed with fixed parameter values. In reality, the relationship between branching and elongation may alter during outgrowth due to changes in intrinsic growth parameters or due to external influences. In summary, our model demonstrates an intrinsic outgrowth scheme that can produce a wide range of different dendritic tree types. In contrast to previous models, all parameters are identifiable with particular neurobiological processes. The aim of the current model is to show how a characteristic branching template may be generated intrinsically by the cell. This template could be modified or altered by environmental influences. At present, the model does not take into account external branching signals. It could be adapted to include the direct effect of external molecules (e.g. chemoattractants) on elongation and branching, or the effects of synaptic interactions of cells in a network. Any synaptic activity will have a significant effect on the calcium signalling pathways and the rate of MAP2 (de)phosphorylation. It is not the aim of the model to suggest that control of the microtubule array through CaMKII phosphorylation of MAP2 is the only possible mechanism involved in dendritic development, either internal or external. However, this model does provide a starting point for investigating how intrinsic factors affect the characteristic dendritic branching patterns of neurons.

Tim Hely thanks the Wellcome Trust for support under a Mathematical Biology Prize Studentship. Bruce Graham is supported by MRC Programme Grant 9119632 to Prof. David Willshaw. Arjen van Ooyen thanks the Wellcome Trust for support under a Wellcome Travelling Research Fellowship. The authors thank both referees for their valuable comments.

REFERENCES

- ALBINET, G. & PELCE, P. (1996). Computer simulation of neurite outgrowth. *Europhys. Lett.* **33**, 569–574.
- AUDESIRK, G., CABELL, L. & KERN, M. (1997). Modulation of neurite branching by protein phosphorylation in cultured rat hippocampal neurons. *Dev. Brain Res.* **102**, 247–260.
- BRAY, D. (1984). Axonal growth in response to experimentally applied mechanical tension. *Dev. Biol.* **102**, 379–389.
- BURKE, R. E., MARKS, W. B. & ULFHAKE, B. (1992). A parsimonious description of motoneuron dendritic morphology using computer simulation. *J. Neurosci.* **12**, 2403–2416.
- DIEZ-GUERRA, F. J. & AVILA, J. (1993). MAP2 phosphorylation parallels dendrite arborization in hippocampal neurones in culture. *NeuroReport* **4**, 412–419.
- DITYATEV, A., CHMYKHOVA, N., STUDER, L., KARAMIAN, O., KOZHANOV, V. & CLAMANN, H. P. (1995). Comparison of the topology and growth rules of motoneuronal dendrites. *J. Comp. Neurol.* **363**, 505–516.
- FRIEDRICH, P. & ASZODI, A. (1991). MAP2: a sensitive cross-linker and adjustable spacer in dendritic architecture. *FEBS Lett.* **295**, 5–9.
- GIESE, K. P., FEDOROV, N. B., FILIPKOWSKI, R. K. & SILVA, A. J. (1998). Autophosphorylation at Thr286 of the alpha calcium-calmodulin kinase II in LTP and learning. *Science* **279**, 870–873.
- GRAHAM, B., HELY, T. A. & VAN OUYEN, A. (1998). An internal signalling model of the dendritic branching process. *European J. Neurosci.* **10S**, 274.
- HALL, G., LEE, V. & KOSIK, K. (1991). Microtubule destabilization and neurofilament phosphorylation precede dendritic sprouting after close axotomy of lamprey central neurons. *Proc. Natl Acad. Sci. U.S.A.* **88**, 5016–5020.
- HANCOCK, J. T. (1997). *Cell Signalling*. Reading, MA: Addison-Wesley Longman Limited.
- HENTSCHEL, H. G. E. & FINE, A. (1996). Diffusion-regulated control of cellular dendritic morphogenesis. *Proc. Roy. Soc. Lond. B* **263**, 1–8.
- KLEE, C. B., DRAETTA, G. F. & HUBBARD, M. J. (1988). Calcineurin. *Adv. Enzymol. Relat. Areas. Mol. Biol.* **61**, 149–200.
- KLIEMANN, W. A. (1987). Stochastic dynamic model for the characterization of the geometrical structure of dendritic processes. *Bull. Math. Biol.* **49**, 135–152.
- KUHN, T. B., WILLIAMS, C. V., DOU, P. & KATER, S. B. (1998). Laminin directs growth cone navigation via two temporally and functionally distinct calcium signals. *J. Neurosci.* **18**, 184–194.
- LARKMAN, A. (1991). Dendritic morphology of pyramidal neurones of the visual cortex of the rat: I. Branching patterns. *J. Comp. Neurol.* **306**, 307–319.
- LEWIS, S. A., IVANOV, I. E., LEE, G. & COWAN, N. (1989). Organization of microtubules in dendrites and axons is determined by a short hydrophobic zipper in microtubule-associated proteins MAP2 and tau. *Nature* **342**, 498–505.
- LI, G.-H., QIN, C.-D. & WANG, Z.-S. (1992). Neurite branching pattern formation: modeling and computer simulation. *J. theor. Biol.* **157**, 463–486.
- MACCIONI, R. & CAMBIAZO, V. (1995). Role of microtubule-associated proteins in the control of microtubule assembly. *Physiol. Rev.* **75**, 835–864.
- MATTSON, M. P. & KATER, S. B. (1987). Calcium regulation of neurite outgrowth and growth cone motility. *J. Neurosci.* **7**, 4034–4043.
- PELCE, P. (1993) Origin of cellular ionic currents. *Phys. Rev. Lett.* **71**, 1107–1110.
- PRESS, W. H., FLANNERY, B. P., TEUKOLSKY, S. A. & VETTERLING, W. T. (1988). *Numerical Recipes in C*. Cambridge: University of Cambridge Press.
- SCHILLING, K., DICKINSON, M., CONNOR, J. & MORGAN, J. (1991). Electrical activity in cerebellar cultures determines Purkinje cell dendritic growth patterns. *Neuron* **7**, 891–902.
- SELDEN, S. C. & POLLARD, T. D. (1983). Phosphorylation of microtubule associated proteins regulate their interaction with actin filaments. *J. Biol. Chem.* **258**, 7064–7071.
- TAMORI, Y. (1993). Theory of dendritic morphology. *Phys. Rev. E* **48**, 3124–3129.
- VALLEE, R. (1980). Structure and phosphorylation of microtubule-associated protein 2 (MAP2). *Proc. Natl Acad. Sci. U.S.A.* **77**, 3206–3210.
- VAN PELT, J. & UYLINGS, H. (1997). Natural variability in the geometry of dendritic branching patterns. In: *Mathematical Modeling in the Neurosciences: from Ionic Channels to Neural Networks* (Poznanski, R. R., ed.), Vol. 41, pp. 1119–1125. Gordon and Breach.
- VAN PELT, J. & VERWER, R. W. H. (1986). Topological properties of binary trees grown with order-dependent branching probabilities. *Bull. Math. Biol.* **48**, 197–211.
- VAN PELT, J., UYLINGS, H. B. M., VERWER, R. W. H., PENTNEY, R. J. & WOLDENBERG, M. (1992). Tree asymmetry—a sensitive and practical measure of binary topological trees. *Bull. Math. Biol.* **54**, 759–784.
- VAN PELT, J., DITYATEV, A. & UYLINGS, H. (1997). Natural variability in the number of dendritic segments: model-based inferences about branching during neurite outgrowth. *J. Comp. Neurol.* **387**, 325–340.
- VAN VEEN, M. & VAN PELT, J. (1992). A model for outgrowth of branching neurites. *J. theor. Biol.* **159**, 1–23.
- VAN VEEN, M. & VAN PELT, J. (1994). Neuritic growth rate described by modelling microtubule dynamics. *Bull. Math. Biol.* **56**, 249–273.
- WELNHOFER, E. A., ZHAO, L. & COHAN, C. S. (1999). Calcium influx alters actin bundle dynamics and retrograde flow in *Helisoma* growth cones. *J. Neurosci.* **19**, 7971–7982.
- YAMAMOTO, H., SAITOH, Y., FUKUNAGA, K., NISHIMURA, H. & MIYAMOTO, E. (1985). Dephosphorylation of microtubule proteins by brain protein phosphatases 1 and 2A, and its effect on microtubule assembly. *J. Neurochem.* **50**, 1614–1623.